

AperTO - Archivio Istituzionale Open Access dell'Università di Torino

Standing adult human phantoms based on 10th, 50th and 90th mass and height percentiles of male and female Caucasian populations

This is a pre print version of the following article:

Original Citation:

Availability:

This version is available <http://hdl.handle.net/2318/2024630> since 2024-10-15T10:12:33Z

Published version:

DOI:10.1088/0031-9155/56/13/002

Terms of use:

Open Access

Anyone can freely access the full text of works made available as "Open Access". Works made available under a Creative Commons license can be used according to the terms and conditions of said license. Use of all other works requires consent of the right holder (author or publisher) if not exempted from copyright protection by the applicable law.

(Article begins on next page)

Standing adult human phantoms based on 10th, 50th and 90th mass and height percentiles of male and female Caucasian populations

(submitted to PMB on March 13, 2011)

V F Cassola¹, F M Milian², R Kramer¹, C A B de Oliveira Lira¹ and H J Khoury¹

¹Department of Nuclear Energy, Federal University of Pernambuco, Avenida Prof. Luiz Freire, 1000, CEP 50740-540, Recife, PE, Brazil

²Department of Exact Science and Technology, State University of Santa Cruz, Campus Soane Nazaré de Andrade, Km 16 Rodovia Ilhéus-Itabuna CEP 45662-000, Ilhéus, BA, Brasil

E-mail: rkramer@uol.com.br

Abstract

Computational anthropomorphic human phantoms are useful tools developed for the calculation of absorbed or equivalent dose to radiosensitive organs and tissues of the human body. The problem is, however, that, strictly spoken, the results can be applied only to a person who has the same anatomy as the phantom, while for a person with different body mass and/or standing height the data could be wrong. In order to improve this situation for many areas in radiological protection, this study developed 18 anthropometric adult human phantoms, nine models per sex, as a function of the 10th, 50th and 90th mass and height percentiles of Caucasian populations. The anthropometric target parameters for body mass, standing height and other body measures were extracted from PeopleSize, a well known software package used in the area of ergonomics. The phantoms were developed based on the assumption of constant body-mass index for a given mass percentile and for different heights. For a given height, increase or decrease of body mass was considered to reflect mainly the change of subcutaneous adipose tissue mass, i.e. that organ masses were not changed. Organ mass scaling as a function of height was based on information extracted from autopsy data. The methods used here were compared with those used in other studies, anatomically as well as dosimetrically. For external exposure the results show that equivalent dose decreases with increasing body mass for organs and tissues located below the subcutaneous adipose tissue layer, like liver, colon, stomach, etc., while for organs located at the surface, like breasts, testes and skin, the equivalent dose increases or remains constant with increasing body mass due to weak attenuation and more scatter radiation caused by the increasing adipose tissue mass. Changes of standing height have little influence on the equivalent dose to organs and tissues from external exposure. Specific absorbed fractions (SAFs) have been calculated with the 18 anthropometric phantoms. The results show that SAFs decrease with increasing height and increase with increasing body mass. The calculated data suggest that changes of the body mass may have a significant effect on equivalent doses primarily for external exposure to organs and tissue located below the adipose tissue layer, while for superficial organs, for changes of the height and for internal exposures the effects on equivalent dose are small to moderate.

1. Introduction

It is well known that organ and tissue absorbed doses determined with a human phantom can be applied to a person, strictly spoken, only if this person has exactly the anatomical characteristics of the phantom. Therefore, the use of phantoms with different body masses and/or standing heights would certainly improve the organ and tissue absorbed dose assessments for populations, like patients, occupationally exposed personnel or members of the public. Attempts to adjust computational phantoms to the variability of body sizes found among real humans began in the early days of phantom development. By increasing the sagittal diameter from 20 to 28 cm, Kramer (1979) simulated pelvic radiographs with the MIRD5 phantom (Snyder et al 1978) and found that organ and tissue absorbed doses normalized to exit air kerma generally increase with increasing thickness. By changing voxel dimensions, Veit and Zankl (1992, 1993) and Zankl et al (2000) varied the diameters of the voxel phantoms BABY, CHILD and GOLEM during simulations of X-ray examinations and got similar results.

Using statistical data from the Finnish clothing industry, the Alderson-Rando phantom (Alderson 1962) and Monte Carlo depth dose distributions calculated in a homogeneous medium, Servomaa et al (1989) and Ranniko et al (1997) developed the software WinODS (2008) that calculates organ and effective doses as a function of sex, body mass and height of persons, which probably was one of the first dose calculation software packages and also the first attempt to use statistical anthropometric data for the development of variable phantoms. Although outdated, the WinODS project represents still an interesting approach to take human body variability into account.

Clairand et al (2000) developed six MIRD5-type phantoms of different heights, three for each sex, based on anthropometric data gathered from autopsies of Caucasian individuals. Application to internal dosimetry revealed a decrease of S values for ^{131}I with increasing height. Addition of adipose tissue layers on the surface of the MIRD5 phantom was used by Kim et al (2003) to study the effect of fat layer thickness on the effective dose, while Tung et al (2008) used the WinODS software and a linear relationship between body mass index (BMI) and the person's thickness to investigate the effect of body size on the effective dose. Kim et al's results showed a decrease of the effective dose with increasing fat layer for radiation incident perpendicular to the phantoms longitudinal axis, while the effective dose increased with increasing fat layer for overhead exposure due to additional scatter in the fat layer. Tung et al reported decrease of the effective dose with increasing BMI.

Using CT images of nine male patients with body masses between 59 and 90 kg, and heights between 162 and 180 cm, Divoli et al (2009) calculated S values for ^{131}I and compared the results with corresponding data given by the OLINDA software (Stabin et al 2005) for a standard patient. The ratios between the standard and the patient-specific S values varied between 0.45 and 2.47.

Apart from body mass and height, also the posture was identified as a parameter influencing organ and tissue absorbed doses (Sato et al 2007, 2008a, b). The shift of internal organs and the change of anthropometric parameters, like sagittal abdominal diameter, lateral diameter, etc. can cause 50-60% differences for organ and tissue equivalent doses in X-ray diagnosis when a patient's posture changes from standing to supine (Cassola et al 2010b).

Recently, phantom developers began constructing libraries of phantoms as a function of anthropometric parameters. The idea is to calculate organ and tissue equivalent dose conversion coefficients (CCs) for a grid of body masses and standing heights and then to linearly interpolate CCs for the actual anthropometric parameters of a person between the next CCs given in the grid, for example. Actually, such phantom libraries could have been developed long time ago based on stylized phantoms because they can be changed quite easily. Still, it is well known that voxel phantoms would anatomically be better suited for such a purpose, but the problem is that voxel phantoms are difficult to change. The deadlocked situation could be overcome by applying 3D modelling software, developed in the area of computer graphics and animated film, to existing voxel phantoms and/or to 3D anatomical or free-form objects to create so-called boundary representation (BREP) phantoms

based on non-uniform rational B-splines (NURBS) and/or on polygon mesh surfaces which can be anatomically highly realistic and flexible at the same time. Pioneered by Segars (2001), who introduced a Cardiac-Torso phantom based on CT images from the Visible Human Project (<http://www.nlm.nih.gov/research/visible>) using NURBS surfaces, numerous BREP phantoms have meanwhile been published based on NURBS and/or polygon mesh surfaces, either representing base phantoms (Lee et al 2007a, b, 2008, Johnson et al 2009a, Jeong et al 2008, Xu et al 2008, Zhang et al 2008a, b, 2009, Cassola et al 2010a), because their organ and tissue masses comply with reference data given by ICRP89 (ICRP 2002), or representing specific phantoms for patients (Li et al 2011) or other persons (Xu et al 2007).

Probably one of the first libraries of human 3D shapes has been developed by Azouz et al (2006) who used anthropometric data from the CAESAR survey (<http://store.sae.org/caesar/>) to make human 3D models available on the Procrustica website (<http://132.246.39.117/>). These 3D models represent only surfaces, i.e. they are not human phantoms with skeletons, organs and tissues and will therefore not be considered here in the comparison with other studies.

A preview on an extended library of phantoms was given by Johnson et al (2009b) with the presentation of 25 different adult male and 15 different paediatric female phantoms, derived from an adult male phantom and from a paediatric female phantom of the UF phantom family (Lee et al 2010), using statistical data from the U.S. NHANES survey (<http://www.cdc.gov/nchs/nhanes.htm>), like standing height, sitting height, body mass and other anthropometric parameters to derive 10th, 25th, 50th, 75th and 90th percentiles for anthropometric parameters of interest.

Also using U.S. NHANES survey data and the RPI-AM and the RPI-AF base phantoms, Na et al (2010) developed 5th, 50th and 95th mass and height percentile male and female adult phantoms. The Na et al study also presents dosimetric calculations for external exposure to photons which show a general increase of organ and tissue absorbed doses with decreasing body mass and height.

The Vanderbilt University reference adult and paediatric phantom series (Stabin et al 2010) was used to develop 10th, 25th, 50th, 75th and 90th height percentile phantoms (Marine et al 2010) and moderately (BMI = 33 kg/m²) as well as severely (BMI = 37 kg/m²) obese phantoms derived from the 50th weight percentile phantom (Clark et al 2010) to study the effect of height and body mass on specific absorbed fractions (SAFs). Apart from other U.S. statistical sources, also NHANES survey data were used in that study. It was found by Marine et al (2010) that SAFs sometimes decrease significantly with increasing height, which confirms the findings by Clairand et al (2000), while the calculations by Clark et al (2010) showed mixed effect of obesity on SAFs.

In the study presented here, a method is proposed that uses statistical anthropometric data from Caucasian male and female adult populations, autopsy results for organ masses and other data from medical investigations to develop 18 anthropometric, standing phantoms, nine for each sex, based on 10th, 50th and 90th percentiles for body mass, standing height, sitting height, chest depth, waist depth, shoulder breadth, hip breadth, waist, arm, thigh and buttock circumferences. The anthropometric phantoms were derived from the standing male base phantom MASH3 and the standing female base phantom FASH3, which comply with the reference data for organ masses, body masses and standing heights given by ICRP89 (ICRP 2002). In order to keep the paper at a reasonable length, some data were moved to a supplementary data file which can also be downloaded from the journal's website. Figures and tables of the supplementary data file are marked with an "S".

2. Materials and methods

2.1 The standing base phantoms MASH3_sta and FASH3_sta

MASH3_sta and FASH3_sta represent the third edition of the mesh-based adult phantoms which were released in early 2010 (Cassola et al 2010a) and then later revised to become the standing MASH2_sta and FASH2_sta phantoms (Cassola et al 2010b). The third edition became necessary because some “holes” were discovered in the walls of gastro-intestinal organs of both phantoms. These “holes” were fixed, although dosimetric consequences have not been observed for all common exposure conditions. Additionally, in the male phantom the distribution of the lymphatic nodes was revised and the position of the prostate gland was anatomically improved. Figures 1a and 1b show the prostate’s position in the standing MASH2_sta and MASH3_sta phantoms, respectively.

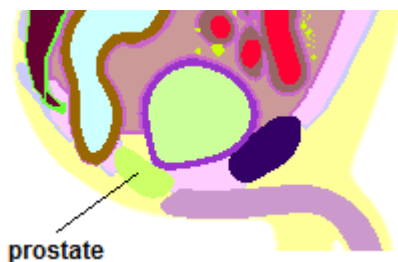


Figure 1a. MASH2_sta prostate

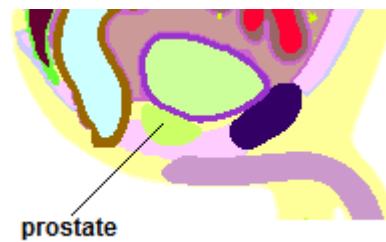


Figure 1b. MASH3_sta prostate



Figure 2a. MASH3_sta phantom



Figure 2b. FASH3_sta phantom

In this study, MASH3_sta and FASH3_sta, shown in figures 2a and 2b, are called ‘base phantoms’ because organ and tissue masses, total body mass and stature (= standing height) correspond to the reference data given by ICRP89 (ICRP 2002). The 18 anthropometric phantoms will be developed by changing the base phantoms MASH3_sta and FASH3_sta using the anthropometric data described in the following sections.

2.2 Definition of Caucasian adult percentile males and females

PeopleSize, available at www.openerg.com, is a commercially available software package widely used in the area of ergonomics. The anthropometric data, which can be extracted from PeopleSize, are based on almost 100 publications, surveys and studies originating from countries in North America, Europe, Asia and Australia, among them also the U.S. NHANES surveys. According to the online manual of PeopleSize, “data are expressed as percentile which is the percentage of people who are smaller in an individual dimension” (www.openerg.com). Following ICRP89 (ICRP 2002), the percentiles extracted from PeopleSize for this study were taken from surveys of countries with predominantly Caucasian populations.

2.2.1 Body mass and standing height

Figure 3 shows how data are extracted from PeopleSize. By clicking on the red arrows in the image on the left, the selected anthropometric parameter pops up in the header of a table. Clicking on “settings” the user can define the population and the percentiles, which are the only parameters used for this study. Ergonomic projects would probably use additional parameters offered by PeopleSize. Figure 3 shows tables for 10th and 50th body mass percentiles for Australian males and 50th and 90th standing height percentiles for German males. 50% of German males have standing heights smaller than 177.1 cm or 10% of Australian males have body masses smaller than 70 kg, for example.

The screenshot displays two side-by-side software windows from PeopleSize. On the left is a diagram of a human figure with red arrows indicating measurement points for weight and stature. The right window is titled 'Measurements FROM percentiles' and is split into two panels: 'Weight' and 'Stature'.

Weight Panel:

Largest User		%ile	
Australian Male 18-64		50th	
Smallest User		%ile	
Australian Male 18-64		10th	
		70	84
Settings...	Adjustments	+	+
Help	(none)		
Export	enter optional item	-0	+0
Hide/Close	Units	Kg	
		70	84

Stature Panel:

Largest User		%ile	
German Male 18-64		90th	
Smallest User		%ile	
German Male 18-64		50th	
		1771	1861
Settings...	Adjustments	+	+
Help	Headgear	1x0	1x0
Help	Footwear	1x0	1x0
Export	enter optional item	-0	+0
Hide/Close	Units	mm	
		1771	1861

Notes for Weight: The person wears light, indoor clothing, a gown, or underwear only, and no shoes. All weight-related data are tuned to the real distribution of weight in Western populations (see Help, Data)

Notes for Stature: Measured vertically from the floor to the highest point of the head, compressing the hair. The person stands erect, looking ahead, the arms relaxed at the sides. The shoulder blades (scapulae) and buttocks will ideally be in contact with a vertical surface.

Figure 3. Screen shot from PeopleSize software used to determine mass and stature (= standing height) percentiles for Australian and German males, respectively

Table 1. 10th, 50th and 90th mass and height percentiles for male and female adults for Caucasian populations from nine countries extracted from PeopleSize. Additionally, average values and data from ICRP89 (ICRP 2002) are shown.

Country	Age group (years)	Body Mass Percentiles						Standing Height Percentiles					
		Female			Male			Female			Male		
		10th (kg)	50th (kg)	90th (kg)	10th (kg)	50th (kg)	90th (kg)	10th (cm)	50th (cm)	90th (cm)	10th (cm)	50th (cm)	90th (cm)
Sweden	18-65	55	63	77	64	77	95	158.7	167.6	176.4	169.5	178.6	187.6
Netherlands	18-64	58	67	84	68	79	94	158.2	166.1	173.9	169.9	179.2	188.6
Germany	18-65	53	66	89	67	81	101	157.1	165.5	173.9	168.0	177.1	186.1
Belgium	18-65	56	67	87	65	78	96	155.9	164.6	173.3	166.9	176.6	186.3
Australia	18-64	55	68	91	70	84	103	155.2	163.2	171.2	167.2	176.0	184.8
USA	over 20	53	71	102	66	85	110	154.4	163.0	171.5	167.2	176.9	186.6
France	18-70	50	60	77	63	75	92	154.2	162.5	170.8	166.7	175.6	184.5
UK	18-64	53	67	90	67	81	100	154.1	162.3	170.6	166.9	175.9	184.9
Italy	18-83	50	57	71	60	73	91	151.6	159.8	167.9	163.2	172.1	181.0
Average		54	65	85	66	79	98	155.5	163.8	172.2	167.3	176.4	185.6
ICRP89			60			73			163.0			176.0	

Table 1 shows 10th, 50th and 90th mass and height percentiles for male and female adults for Caucasian populations from nine countries extracted from PeopleSize. Additionally, average values for each mass or height percentile and the corresponding body masses and standing heights from ICRP89 (ICRP 2002) are presented. Differences between 10th and 50th standing height percentiles are quite similar to the differences between 50th and 90th standing height percentiles, which reflect a normal distribution, while corresponding data for the body mass indicate a skewed distribution. In general, among anthropometric data one usually finds normal distributions for dimensions, like standing or sitting height, arm or leg length, shoulder to grip distance, etc., while so-called “fatty” dimensions, like body mass, hip, waist, arm, thigh circumferences, etc., usually show distributions skewed towards the “fatty” end of the distribution.

ICRP89’s standing heights compare well with the average 50th male and female height percentiles, while differences of 5 kg and 6 kg can be observed for the female and male body masses, respectively, between ICRP89 values and the average 50th percentiles. Is ICRP89 therefore wrong with respect to the reference body masses? The answer is: No and Yes! No, because on page 9, paragraph (11), ICRP89 clearly states that the reference values are not representative for “a well-defined population group”, i.e. that they do not represent mean or median values in the statistical sense. They are, however, in some way average values for the data considered by ICRP. Therefore, reference data given by ICRP89 do not represent 50th percentiles for populations from specific countries or for a population averaged over many countries. Yes, because the body mass percentiles from nine countries shown in table 1 reflect a world-wide trend of body mass increase, i.e. that an update of ICRP89 body masses based on more recent data on adipose distribution would probably lead to an increase of the reference male and female adult body masses for Caucasians.

Based on the average data shown in table 1, body masses and standing heights for 18 standing adult males and females have been defined and are shown in table 2, nine for each sex. Central females and males (m50_h50) are those having the average 50th percentile body masses and standing heights, shown in bold characters in table 2. Consequently, the central female has a body mass of 65 kg and a standing height of 163.8 cm, while corresponding data for the central male are 79 kg and 176.4 cm. Using data from table 1, for the 50th standing height percentiles one can now define 10th and

90th mass percentile males and females, called (m10_h50) and (m90_h50), respectively, which are just slimmer and fatter versions of the central males and females, with body masses of 54 and 85 kg for the females and 66 and 98 kg for the males. The last row in table 2 shows the BMIs calculated for h50 males and females. Next, the average 10th and 90th standing height percentiles from table 1 are assigned to the h10 and h90 males and females shown in the first and in the third row of table 2, respectively. Based on the assumption of constant BMI, the body masses for the h10 and h90 males and females have been determined using the BMIs calculated for the 50th height males and females and the average 10th and 90th standing heights percentiles from table 1. In anthropometric surveys body masses and standing heights are usually not correlated, i.e. that a person with 50th percentile body mass can have any standing height or with a 50th percentile standing height can have any body mass, for example. In other words, many combinations of body mass and standing height are possible and one therefore has to come to a reasonable decision on how to define representative adult percentile males and females, here by using the BMI. Apart from body mass and standing height, additional anthropometric parameters were used for the modelling of the phantoms which are shown in tables S1 and S2 of the supplementary data file. The method used to define the body masses and standing heights of the percentile males and females shown in table 2 is partly applying criteria and techniques similar to the methods developed by others. A comprehensive comparison of this and other “modelling philosophies” is presented in a special section in the supplementary data file.

Table 2. Body masses and heights defined for 18 standing adult percentile males and females

Percentil	FEMALE ADULT			MALE ADULT		
	MASS 10th	MASS 50th	MASS 90th	MASS 10th	MASS 50th	MASS 90th
HEIGHT 10th	48.6 kg 155.5 cm m10_h10	58.5 kg 155.5 cm m50_h10	76.7 kg 155.5 cm m90_h10	59.3 kg 167.3 cm m10_h10	71.1 kg 167.3 cm m50_h10	88.2 kg 167.3 cm m90_h10
		↑			↑	
HEIGHT 50th	54 kg 163.8 cm m10_h50	65 kg 163.8 cm m50_h50	85 kg 163.8 cm m90_h50	66 kg 176.4 cm m10_h50	79 kg 176.4 cm m50_h50	98 kg 176.4 cm m90_h50
		↓			↓	
HEIGHT 90th	59.6 kg 172.2 cm m10_h90	71.8 kg 172.2 cm m50_h90	94 kg 172.2 cm m90_h90	73.0 kg 185.6 cm m10_h90	87.5 kg 185.6 cm m50_h90	108.5 kg 185.6 cm m90_h90
BMI (kg/m ²)	20.1	24.2	31.7	21.2	25.4	31.5

2.2.2 Organ and tissues masses as a function of height

De la Grandmaison et al (2001) have determined organ masses in 684 autopsies of adult Caucasian individuals and among other data the study presents a table which correlates organ masses to height. Using this data, 3D scaling factors h90/h50 and h10/h50 for organ masses have been calculated and are presented in table 3 for males and females to be applied to the modelling of organs as a function of height. Information on the relationship between brain mass and height was found in a study by Hartmann et al (1994). The authors investigated brain masses in adults as a function of age, sex, stature and body mass. With respect to height it was found that the brain mass of adult males and females changes by approximately 4 g per cm of height.

Table 3. 3D scaling factors for organ masses derived from autopsy data (de la Grandmaison et al 2001)

Organ	male	male	female	female
	h90/h50	h10/h50	h90/h50	h10/h50
Heart	1.058	0.956		
Right lung	1.186	0.986	1.095	0.906
Left lung	1.194	0.949	1.040	0.953
Liver	1.119	0.889	1.086	0.852
Spleen	1.200	0.800	1.151	0.878
Pancreas	1.028	0.965	1.131	0.910
Right kidney	1.067	0.955	1.080	0.854
Left kidney	1.067	0.945	1.088	0.882
Thyroid	1.000	1.000	1.111	
Average	1.102	0.938	1.098	0.891

In order to cross-check the data of de la Grandmaison et al (2001) and of Hartmann et al (1994), information from a study by Heymsfield et al (2007) was used. Heymsfield et al (2007) suggest that the male brain mass scales with height^{0.83} and the male liver mass with height^{2.65}. Based on Heymsfield et al's formulas on finds for the 90th and 50th male height percentiles for the liver a scaling factor of $1.856^{2.65}/1.764^{2.65} = 1.14$, which agrees with the 1.12 for the male liver in table 3 within a margin of 2%. The height difference between male h90 and h50 is 185.6 cm – 176.4 cm = 9.2 cm. According to Hartmann et al (1994) this would imply a difference of the brain mass of 36.8 g. The brain scaling factor according to Heymsfield et al (2007) is $1.856^{0.83}/1.764^{0.83} = 1.043$. Using the ICRP89 male brain mass of 1450 g for h50, one finds for the h90 brain mass according to Hartmann et al (1994) 1486.8 g and according to Heymsfield et al (2007) 1512.4 g, which shows agreement within a margin of 1.7%.

For both sexes, the scaling factors derived from the heights given in table 2 are 0.95 between h10 and h50 and 1.05 between h90 and h50 for the vertical body axis (= z axis), which can be used to calculate the 1D scaling factors in x and y direction. For the liver one would get 1D scaling factors for x and y according to SQRT (1.119/1.05) = 1.03 for the change from h50 to h90, for example. For the skeleton and for organs not mentioned in table 3, excluding the brain, the average 3D scaling factors from table 3 were used. For the female heart the male scaling factors were used, masses of the testes, the ovaries and of the thyroids for both sexes were not changed.

2.3 Modelling of the anthropometric phantoms

Based on the data presented in the previous section and using the 3D modelling software Blender (<http://www.blender.org>), the anthropometric phantoms have been developed as follows:

- a) The body masses of the base phantoms MASH3_sta and FASH3_sta were increased by adding 6 kg and 5 kg, respectively, of subcutaneous adipose tissue, observing the average 50th percentiles for the “fatty” dimensions given in tables S1 and S2. Also, the heights of the base phantoms were increased by 8 mm each. The new phantoms were called **MSTA_m50_h50** and **FSTA_m50_h50** and represent the central phantoms, shown with bold characters in the scheme of table 2.

- b) By reducing or increasing adipose tissue in the MSTA_m50_h50 and in the FSTA_m50_h50 phantoms, the phantoms MSTA_m10_h50, FSTA_m10_h50 and MSTA_m90_h50, FSTA_m90_h50, respectively, were modelled observing the 10th and 90th percentiles of the “fatty” dimensions given in tables S1 and S2. For the modelling of the m10 phantoms additionally muscle and/or soft tissue was reduced in case that the reduction of the adipose tissue did not yield the targeted body mass. Organ masses did not change, based on the assumption that a person’s loss or gain of total body mass reflects decrease or increase of mainly adipose tissue and to a lesser extent also muscle and soft tissue. In table 2, this modelling step is represented by the arrows directing to the right and to the left from the central phantoms m50_h50.
- c) The modelling of the h10 and the h90 phantoms, symbolized in table 2 by the arrows directing up and down, was also based on the central phantoms. Using the 10th and the 90th sitting height percentiles from tables S1 and S2 and the scaling factors plus other information provided in section 2.2.2 the anthropometric phantoms MSTA/FSTA_m50_h10 and m50_h90 were modelled. According to the height ratios, the skeletons were scaled in z direction with 1.05 and with 0.95 for h90 and for h10, respectively. After the scaling of organs, the volumes of soft, muscle and adipose tissue were increased or reduced until the targeted body mass was reached.
- d) Finally, the phantoms MSTA/FSTA_m10_h10, m90_h10, m10_h90 and m90_h90 were modelled based on MSTA/FSTA_m50_h10 and m50_h90 with a procedure similar to the one described under b) and symbolized in table 2 by the arrows directing to the left and to the right from the m50_h10 and the m50_h90 phantoms.

3. Results

3.1 Anatomies of the anthropometric phantoms

3.1.1 Organ and tissue masses

Male and female organ and tissue masses are shown in tables S3 and S4, respectively, of the supplementary data file for the ICRP89 reference adults, the standing adult base phantoms MASH3 and FASH3 and the standing anthropometric adult phantoms MSTA and FSTA for 10th, 50th and 90th height and mass percentiles. For given standing height, mainly adipose tissue and to some extent muscle and soft tissue change as a function of the total body mass, while organ masses and the skeleton mass remain constant which is a consequence of the assumption made under item b) in the previous section. Figure 4 shows male adult adipose tissue masses of the anthropometric phantoms taken from table S3 as a function of the BMI for 10th, 50th and 90th height percentiles. Similar data taken from table S4 are presented in figure 5 for the female adult anthropometric phantoms. In the anthropometric model presented here, the increase or decrease of adipose tissue mass is the main contributor to changes of the BMI or total body mass, with the adult females showing usually higher adipose tissue masses than adult males, a fact already seen for the ICRP89 reference adults.

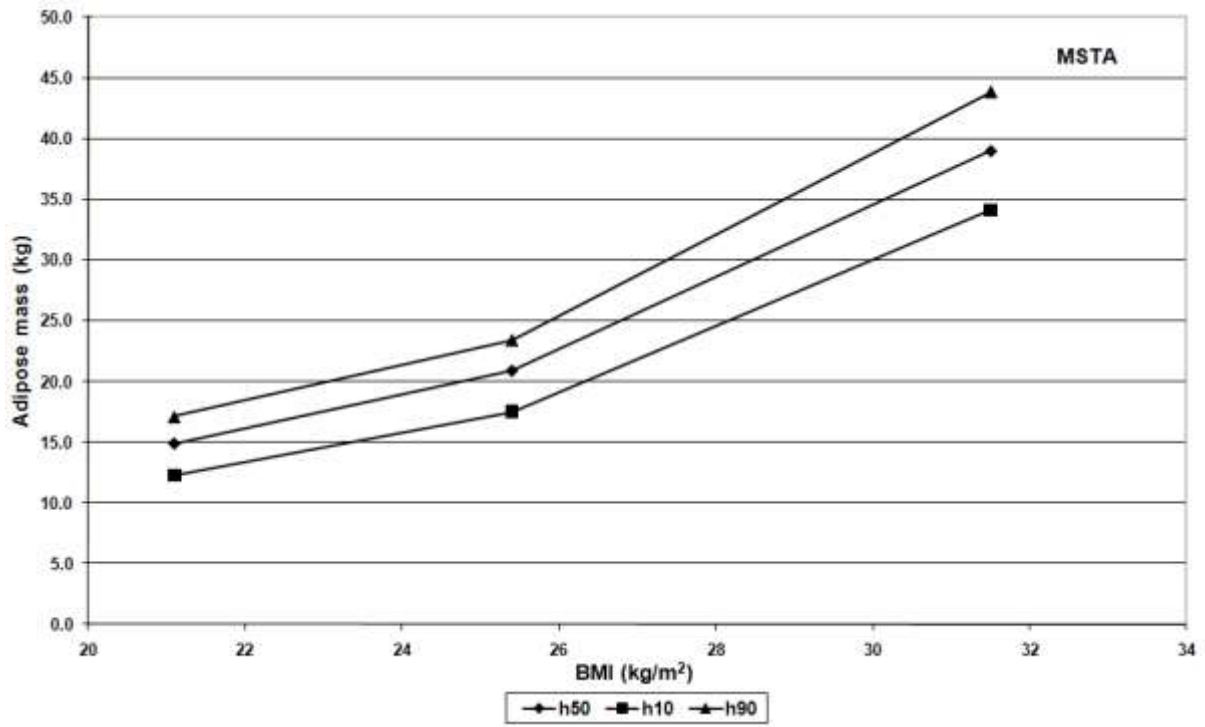


Figure 4. Male adult adipose tissue masses as a function of the body mass index (BMI) for 10th, 50th and 90th height percentiles

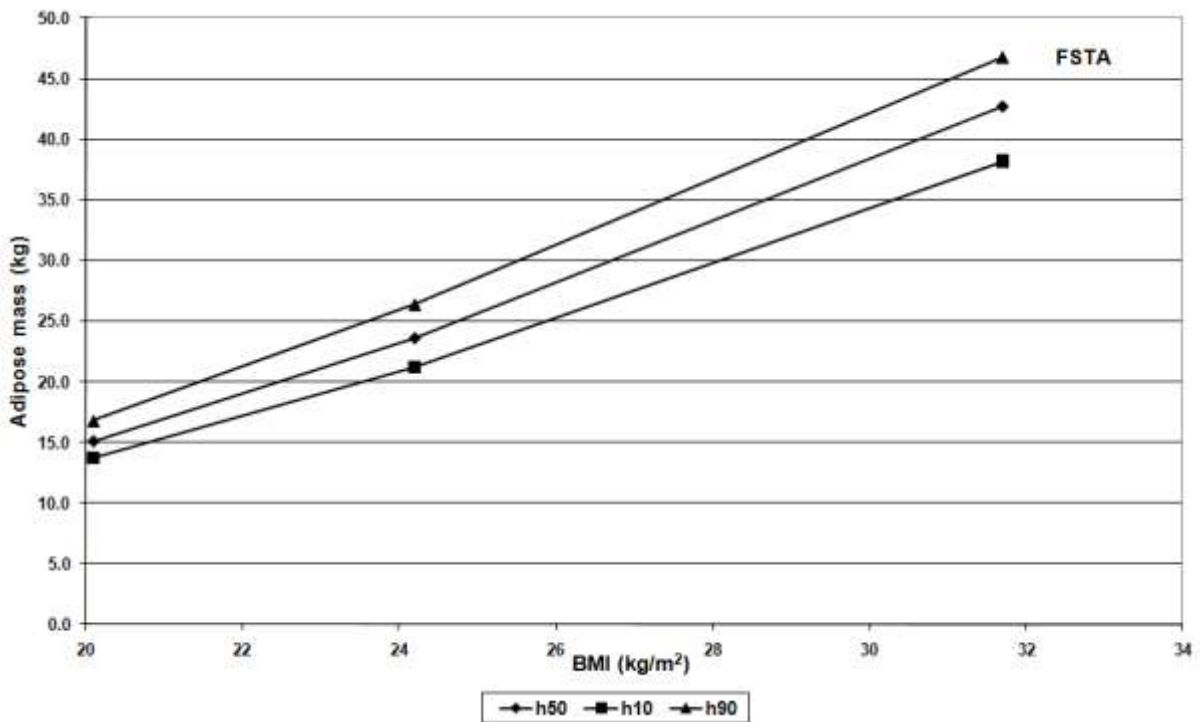


Figure 5. Female adult adipose tissue masses as a function of the body mass index (BMI) for 10th, 50th and 90th height percentiles

Ratios between organ masses of the anthropometric phantoms for the different standing heights are shown in tables 4 and 5, respectively. Apart from some rounding errors, the ratios agree well with those given in table 3. Exceptions are the female heart masses for which the male scaling factors were used, and the female thyroid masses which were left unchanged like in the case of the male thyroids. Also, the masses of the ovaries and the testes were not changed as a function of the height.

Table 4. MSTA organ mass ratios between 90th and 50th and 10th and 50th male height percentiles

MSTA ORGAN / TISSUE	h50 [g]	h10 [g]	h90 [g]	h90/h50 Ratio	h10/h50 Ratio
Adrenals	14.0	13.1	15.5	1.107	0.936
Oesophagus	40.0	37.5	44.1	1.103	0.938
Stomach wall	150.0	140.6	165.3	1.102	0.937
Small Intestine wall	650.0	609.8	716.4	1.102	0.938
Colon wall	370.0	347.0	407.8	1.102	0.938
Liver	1800.0	1600.2	2014.2	1.119	0.889
Gallbladder wall	10.0	9.4	11.0	1.100	0.940
Pancreas	140.0	135.1	143.9	1.028	0.965
Brain	1450.0	1413.6	1488.7	1.027	0.975
Breasts, glandular	10.0	9.4	11.0	1.100	0.940
Heart wall	330.0	315.5	349.1	1.058	0.956
Lungs	1200.0	1160.5	1427.4	1.190	0.967
Spleen	150.0	120.0	179.9	1.199	0.800
Thymus	25.0	23.5	27.6	1.104	0.940
Thyroid	20.0	20.0	20.0	1.000	1.000
Kidneys	310.0	294.5	330.8	1.067	0.950
Bladder wall	50.0	46.9	55.1	1.102	0.938
Testes	35.0	35.0	35.0	1.000	1.000
Prostate	17.0	16.0	18.7	1.100	0.941

Table 5. FSTA organ mass ratios between 90th and 50th and 10th and 50th female height percentiles

FSTA ORGAN / TISSUE	h50 [g]	h10 [g]	h90 [g]	h90/h50 Ratio	h10/h50 Ratio
Adrenals	13.0	11.6	14.3	1.100	0.892
Oesophagus	35.0	31.2	38.4	1.097	0.891
Stomach wall	140.0	124.7	153.7	1.098	0.891
Small Intestine wall	600.0	534.6	658.8	1.098	0.891
Colon wall	360.0	320.7	395.3	1.098	0.891
Liver	1400.0	1192.8	1520.4	1.086	0.852
Gallbladder wall	8.0	7.1	8.8	1.100	0.888
Pancreas	120.0	109.2	135.7	1.131	0.910
Brain	1300.0	1265.1	1337.8	1.029	0.973
Breasts, glandular	200.0	178.2	219.6	1.098	0.891
Heart wall	250.0	222.7	264.5	1.058	0.891
Lungs	950.0	883.0	1014.1	1.067	0.929
Spleen	130.0	114.2	149.7	1.152	0.878
Thymus	20.0	17.8	22.0	1.100	0.890
Thyroid	17.0	17.0	17.0	1.000	1.000
Kidneys	275.0	238.7	298.1	1.084	0.868
Bladder wall	40.0	35.6	44.0	1.100	0.890
Ovaries	11.0	11.0	11.0	1.000	1.000
Uterus	80.0	71.3	87.8	1.098	0.891

3.1.2 Images

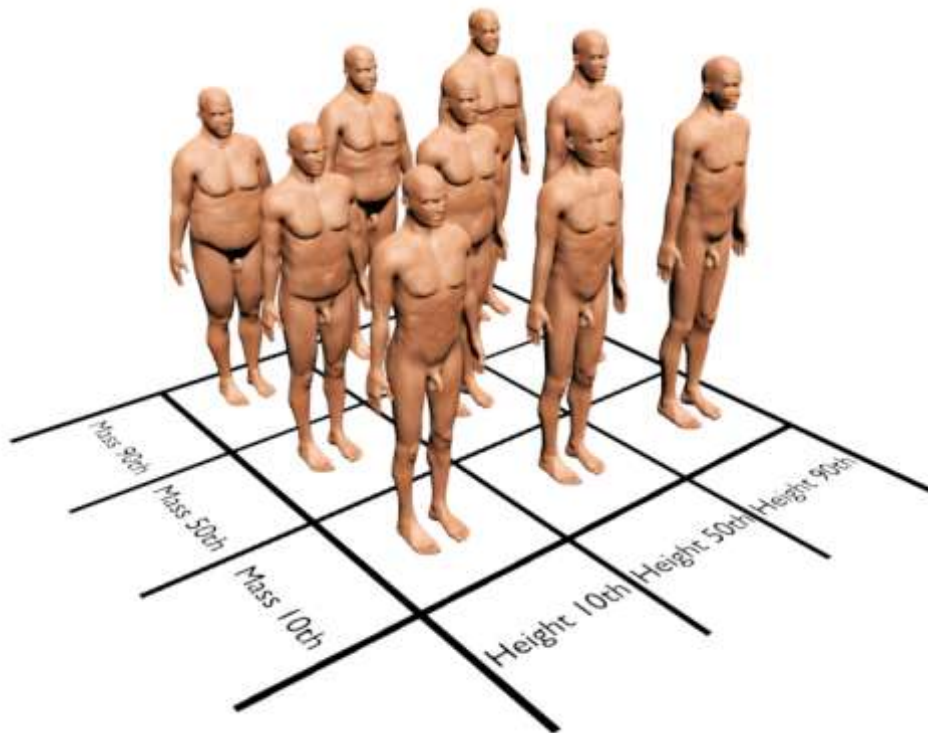


Figure 6. Male anthropometric mesh phantoms for 10th, 50th and 90th mass and height percentiles

Figures 6 and 7 present images of the nine male and nine female anthropometric standing mesh phantoms as a function of the 10th, 50th and 90th mass and height percentiles, respectively. The perspective was chosen to allow for a view of the whole group of the nine phantoms together. Additional images of the phantoms are presented in figures S2 and S3 in the supplementary data file.



Figure 7. Female anthropometric mesh phantoms for 10th, 50th and 90th mass and height percentiles

3.2 Dosimetry

This section will show how body mass and/or standing height may influence dosimetric results. The 18 anthropometric male and female standing mesh phantoms were voxelized and connected to the EGSnrc Monte Carlo (MC) code, version V4-2.3.1, released on February 19, 2010 and available at <http://irs.inms.nrc.ca/software/egsnrc/>. EGSnrc is one of the best bench-marked MC codes for coupled photon/electron transport with a dynamic range of charged particle kinetic energies between a few tens of keV and a few hundred GeV, and of photon energies between 1 keV and several hundred GeV. All EGSnrc transport parameters and cross section options were left at their default values, which are set to achieve the best accuracy EGSnrc is capable of. The coupling of the phantoms to the MC code was using the same methods already applied to the MASH and the FASH base phantoms (Kramer et al 2010). The skeletons of all phantoms were segmented into cortical bone, spongiosa, medullary yellow bone marrow and cartilage to allow for the use of μ CT images of trabecular bone for skeletal dosimetry. Organ and tissue equivalent doses were calculated for a variety of exposure scenarios, two of which will be presented here: External whole body exposure anterior-posterior (AP) to a parallel beam of photons and internal exposure to gamma emitters concentrated in selected organs. Cut-off energies were 2 keV for photons in all tissues, 20 keV for electrons in tissues outside the skeleton and 5 keV in skeletal tissues. Statistical errors were normally well below 1% or below 5% for incident photon energies below 20 keV.

3.2.1 External whole body exposure to photons

In case of external exposure to ionizing radiation, the subcutaneous adipose tissue layer attenuates the incident primary radiation and thereby reduces the equivalent dose for tissues located below that layer, but at the same time also gives rise to scatter radiation which increases the equivalent dose. Organ or tissue equivalent dose is a net result of the two components and, for a given exposure scenario, therefore depends on the size and the location of an organ or tissue relative to the adipose tissue layer. Most of the organs and tissues considered by the ICRP as being radiosensitive (ICRP 2007) are located below the adipose tissue layer. Figure 8 shows that for the MSTA_h50 phantoms exposed to photon radiation AP changes of the body mass from 10th to 50th and to 90th mass percentile has a significant effect on the equivalent dose to the colon wall which is located below the adipose tissue layer. With increasing adipose tissue mass the attenuation of the primary radiation more than compensates the increase of scatter equivalent dose caused by the greater adipose tissue volume, i.e. that the net result for the colon wall is a decrease of equivalent dose. The difference between the equivalent doses to the colon wall for the m10 and m90 phantoms shown in figure 8 is a factor of 10.4 for 20 keV and decrease to 5.5% at 10 MeV. The average difference over the whole energy range is 94% . Figure 8 is representative for all organs and tissues located below the subcutaneous adipose layer, i.e. that increase of body mass leads to a decrease of organ or tissue equivalent dose.

However, some organs or tissues are located at the surface of the body outside the adipose tissue layer, like the breasts with their glandular tissue, the testes and the skin or are located in regions where changes of the adipose tissue layer is small, like the thyroid or the brain. Figure 9 shows that for the FSTA_h90 phantoms exposed to photon radiation AP changes of the body mass from 10th to 50th and to 90th mass percentile has quite a different effect on the equivalent dose to the glandular tissue of the breasts. For the 10th and the 50th mass percentiles phantoms the equivalent doses to the glandular tissues are mostly equal and in the energy range around 70 keV the 50th percentile equivalent dose is even greater than the 10th percentile equivalent dose which is the energy range of maximum backscatter and although, according to table S4, the m50 breasts contain more adipose tissue.

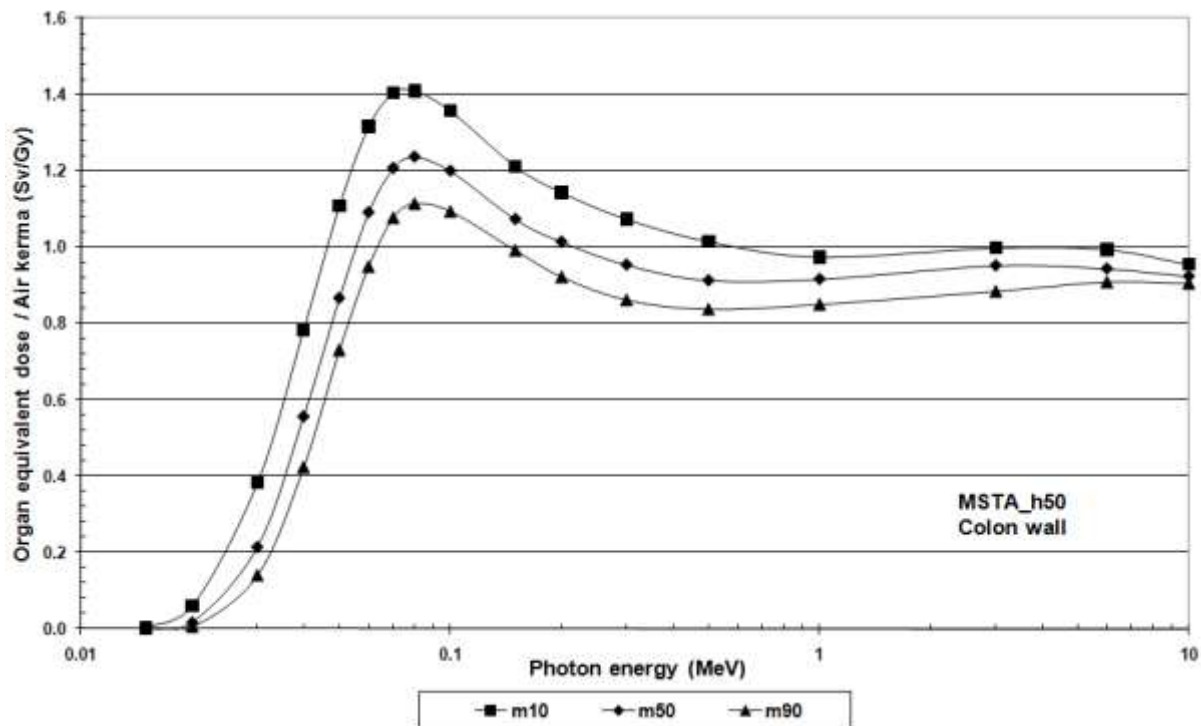


Figure 8. Equivalent dose to the colon wall normalized to air kerma for anterior-posterior exposure with a parallel beam of photons covering the whole body of the male anthropometric phantoms MSTA_m10_h50, MSTA_m50_h50 and MSTA_m90_h50 as a function of the photon energy.

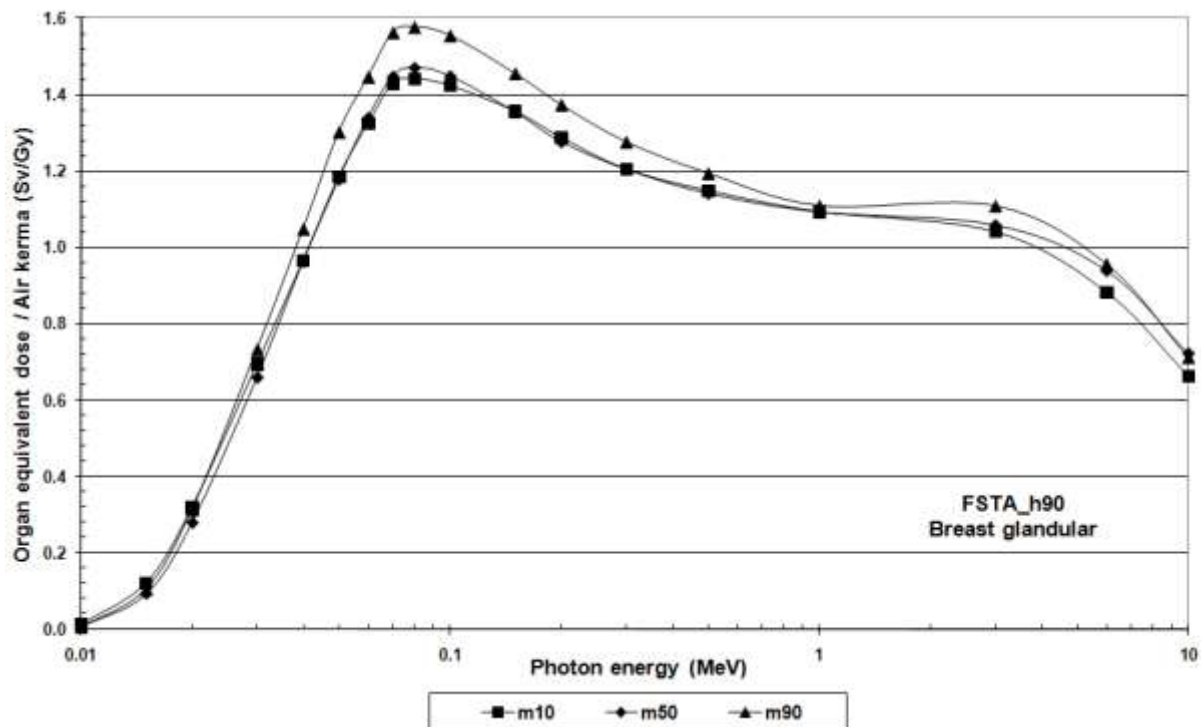


Figure 9. Equivalent dose to the glandular tissue normalized to air kerma for anterior-posterior exposure with a parallel beam of photons covering the whole body of the male anthropometric phantoms FSTA_m10_h90, FSTA_m50_h90 and FSTA_m90_h90 as a function of the photon energy.

Figures 10 a-c show transverse images of the breast regions in the FSTA_m10_h90, m50_h90 and m90_h90 phantoms. More adipose tissue between the breasts of the FSTA_m50_h90 phantom in figure 10 b causes more back and lateral scatter equivalent dose for energies around 70 keV. The equivalent dose to the 90th mass percentile glandular tissue shows the greatest values caused by back and lateral scattered radiation from the thicker subcutaneous adipose layer which can be observed in figure 10 c, although breast adipose tissue is also increasing according to table S4. Similar effects were found for the testes where the adipose tissue mass of the thighs and the lower abdomen of the 90th percentile phantom increase the backscatter equivalent dose and also for the skin because especially for 90th mass percentile phantoms the additional back scatter contribution from more adipose tissue mass more than compensates increased attenuation by the greater body diameter.



Figure 10a. Transverse image of the FSTA_m10_h90 phantom in the breast region. Glandular tissue of the breasts is shown with green colour, adipose breast tissue with violet colour and subcutaneous adipose tissue in yellow.



Figure 10b. Transverse image of the FSTA_m50_h90 phantom in the breast region. Glandular tissue of the breasts is shown with green colour, adipose breast tissue with violet colour and subcutaneous adipose tissue in yellow. More adipose tissue is located between the breasts compared to figure 10 a.



Figure 10c. Transverse image of the FSTA_m90_h90 phantom in the breast region. Glandular tissue of the breasts is shown with green colour, adipose breast tissue with violet colour and subcutaneous adipose tissue in yellow. More adipose tissue is located between and behind the breasts compared to figures 10 a and b.

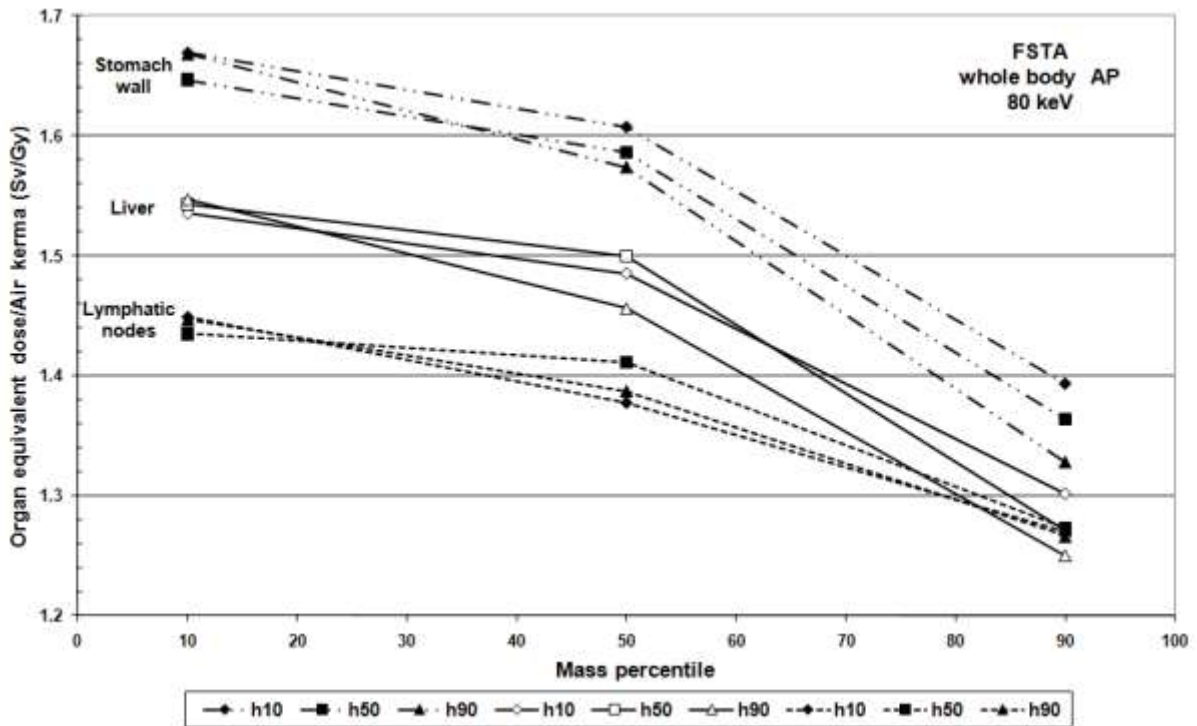


Figure 11. Equivalent dose to the stomach wall, the liver and the lymphatic nodes normalized to air kerma for anterior-posterior exposure with a parallel beam of 80 keV photons covering the whole body of the female anthropometric phantoms FSTA as a function of mass percentiles for different height percentiles

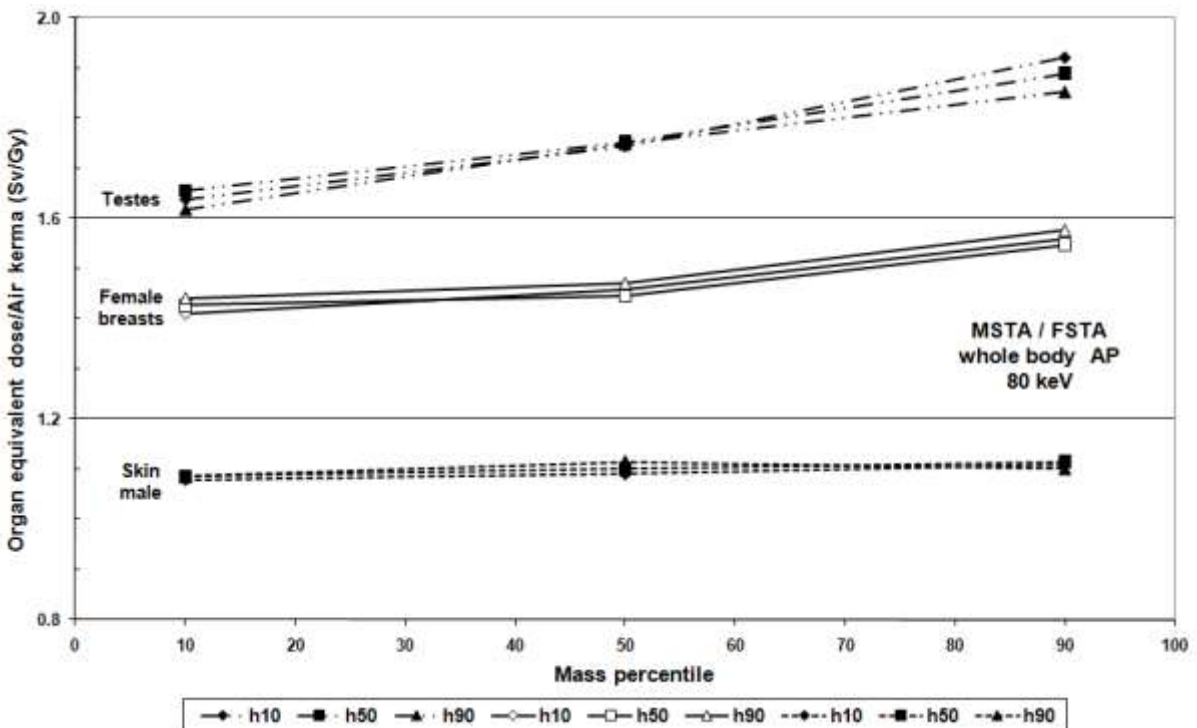


Figure 12. Equivalent dose to the testes, female breasts (glandular tissue) and male skin normalized to air kerma for anterior-posterior exposure with a parallel beam of 80 keV photons covering the whole body of the anthropometric phantoms MSTA and FSTA as a function of mass percentiles for different height percentiles

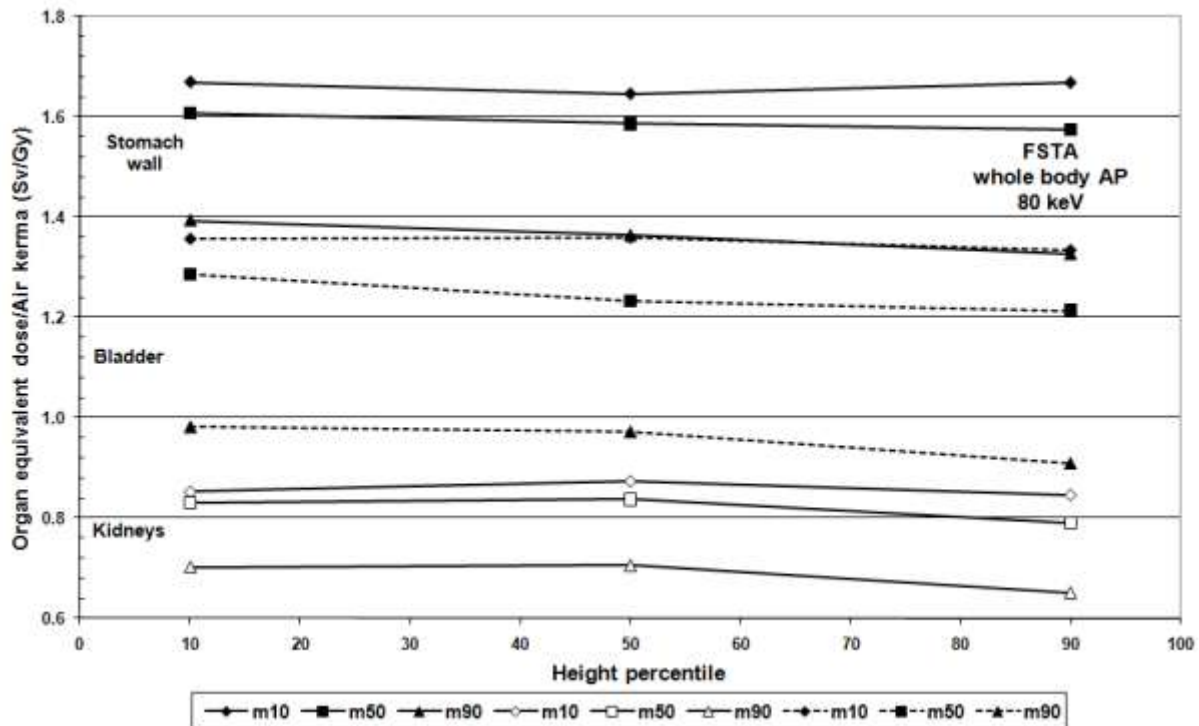


Figure 13. Equivalent dose to the stomach wall, the bladder and the kidneys normalized to air kerma for anterior-posterior exposure with a parallel beam of 80 keV photons covering the whole body of the female anthropometric phantoms FSTA as a function of height percentiles for different mass percentiles

For 80 keV incident photon energy, figure 11 presents equivalent doses to the stomach wall, the liver and the lymphatic nodes as a function of the body mass for different body heights. Figure 12 presents the same quantities for the testes, the female breasts (glandular tissue) and the male skin. Figure 11 shows equivalent doses decreasing by up to 20% with increasing body mass due to the attenuation of the primary radiation which confirms what usually is reported about the effect of increasing body mass on organ and tissue equivalent doses. For low energy photons, diagnostic X-rays with average energy of about 40 keV, for example, the decrease of organ equivalent dose with increasing body mass can be much greater as was shown in figure 8. However, the results of this study also indicate that according to figures 9 and 12 there are organs and tissues located at the surface of the body for which the equivalent dose increases or remains constant with increasing body mass due to increasing backscatter equivalent dose. Compared to body mass, standing height has only little effect on organ and tissue equivalent doses for external whole body exposure. Figure 13 shows equivalent doses to the stomach wall, the bladder and the kidneys as a function of the standing height for different body masses for AP incidence. The differences between equivalent doses for different height percentiles shown in figure 16 are all smaller than 6%. A clear trend of either increasing or decreasing equivalent doses with height for the organs shown in figure 13 could not be observed.

3.2.2 Internal exposure to photons

Specific absorbed fractions in the liver of the MSTA_m50 phantoms when the neighbouring lungs are the source organ SAF(liver←lungs) are shown in figure 14 as a function of the emitted photon energy for the 10th, 50th and 90th height percentiles. The SAFs decrease with increasing height. The maximum differences between h50 and h10 and between h90 and h50 are 1.6% and 12.7%, respectively. Figure 15 shows similar SAFs for the MSTA_h50 phantoms for the 10th, 50th and 90th

mass percentiles. Here the SAFs increase with increasing mass and the maximum differences are 4.8% and 5.3% between m50 and m10 and between m90 and m50, respectively in the energy range between 50 keV and 500 keV.

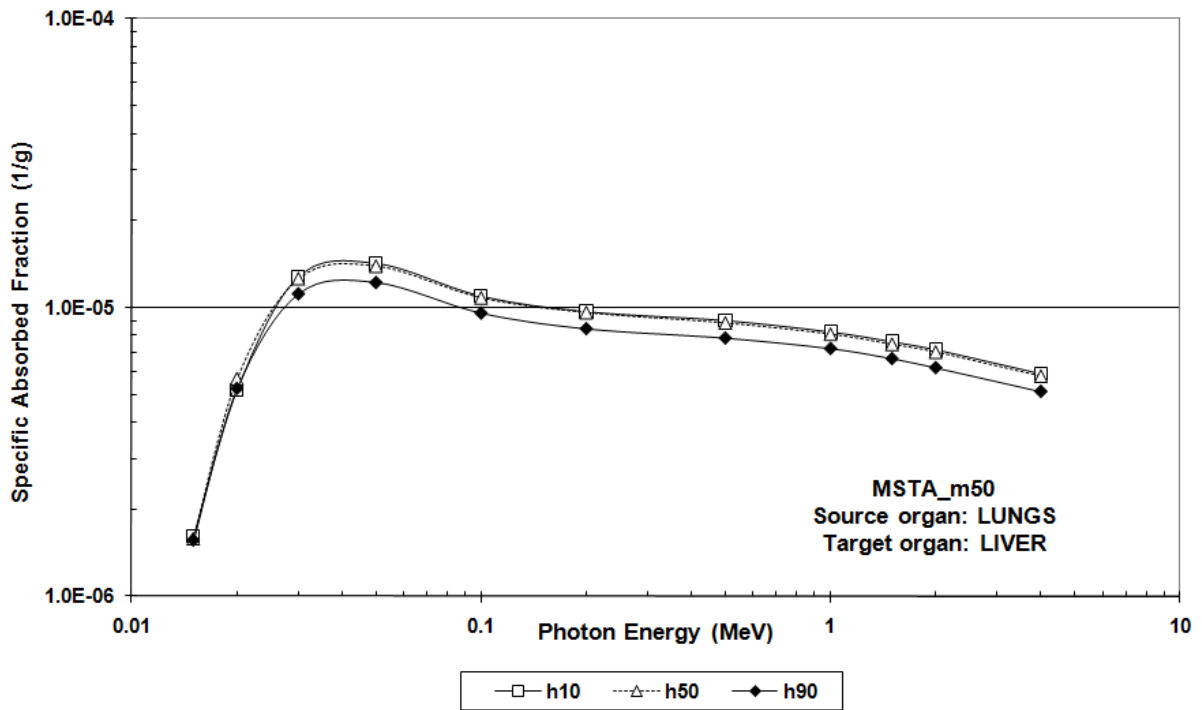


Figure 14. SAF(liver←lungs) as function of the emitted photon energy in the anthropometric phantoms MSTA_m50 for 10th, 50th and 90th height percentiles.

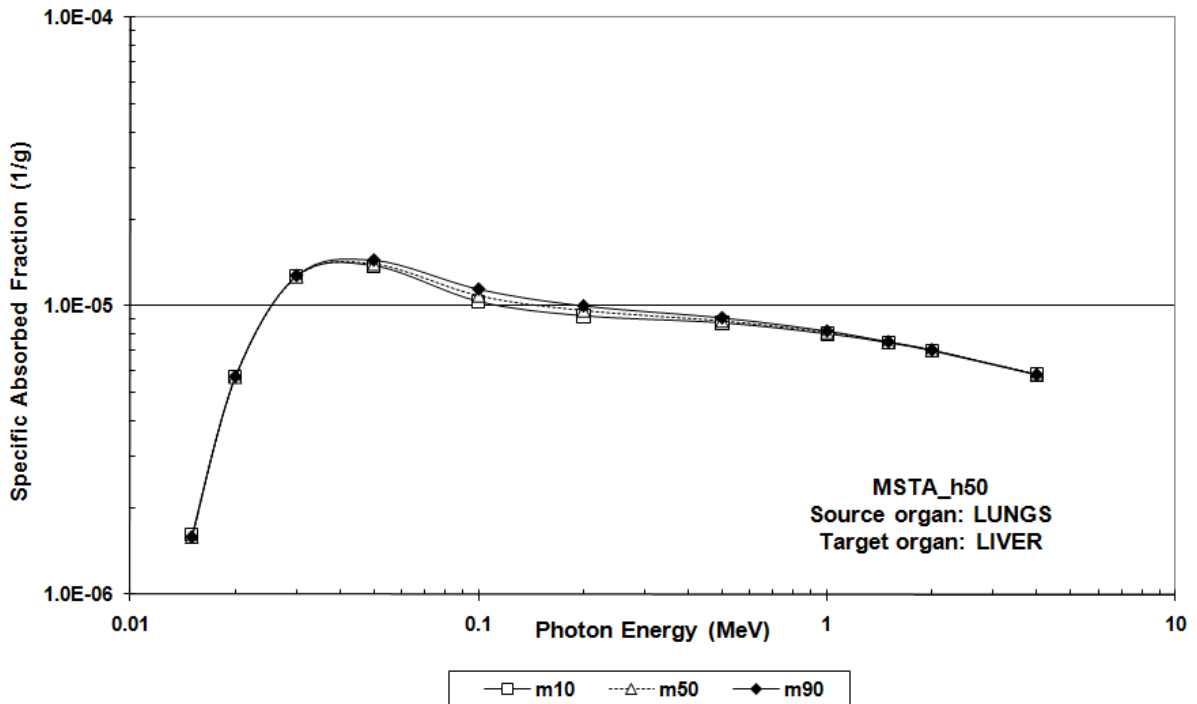


Figure 15. SAF(liver←lungs) as function of the emitted photon energy in the anthropometric phantoms MSTA_h50 for 10th, 50th and 90th mass percentiles.

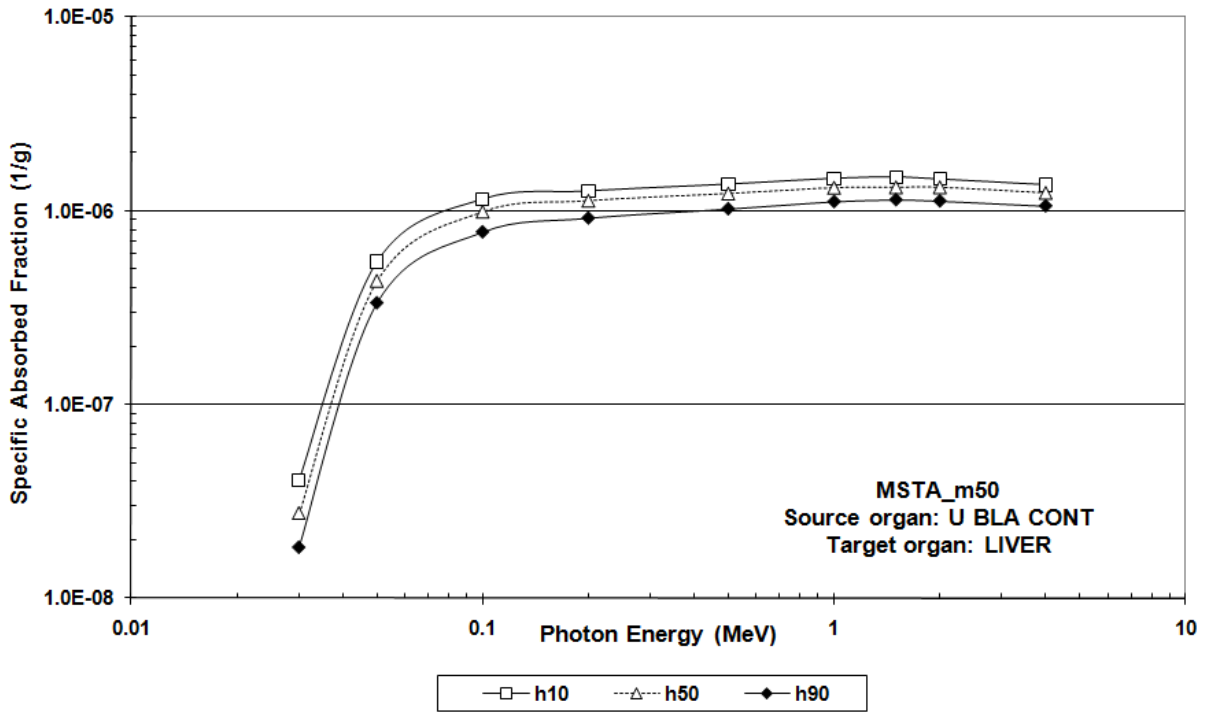


Figure 16. SAF(liver←UBC) as function of the emitted photon energy in the anthropometric phantoms MSTA_m50 for 10th, 50th and 90th height percentiles.

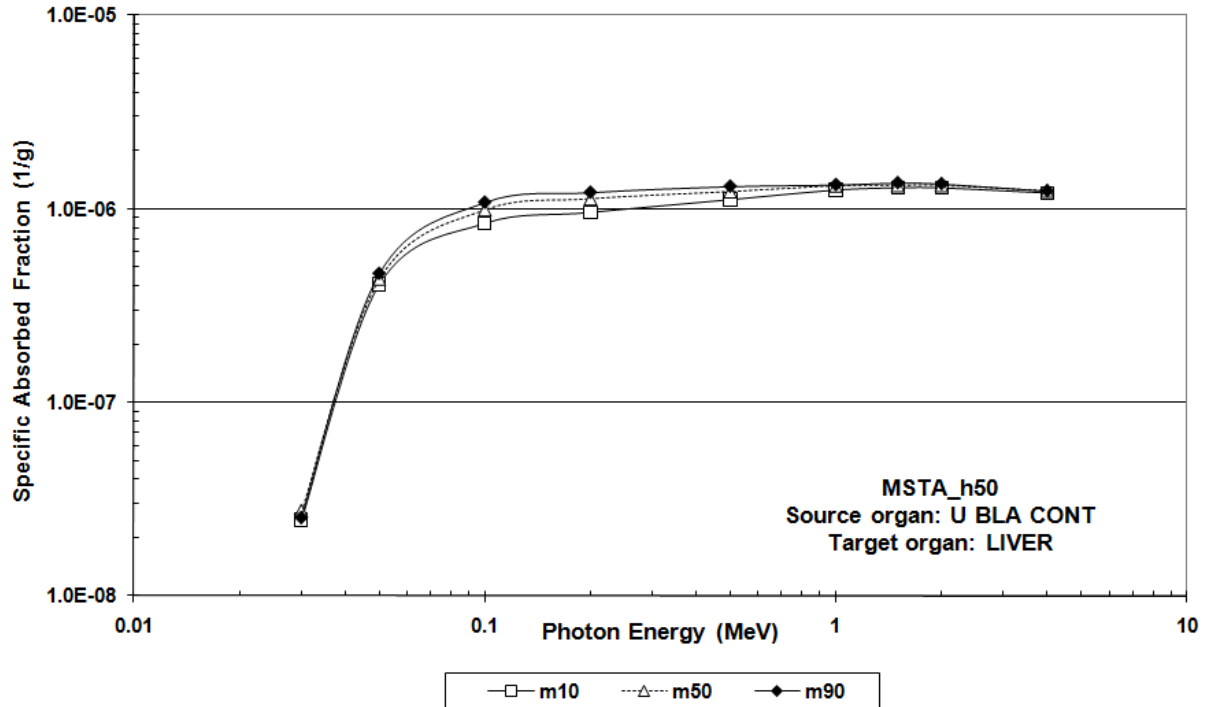


Figure 17. SAF(liver←UBC) as function of the emitted photon energy in the anthropometric phantoms MSTA_h50 for 10th, 50th and 90th mass percentiles.

Figures 16 and 17 show similar SAFs again for the target organ liver but now the source organ is the urinary bladder contents (UBC). The decrease of the height-dependent SAFs in figure 16 reaches 32.7 and 32.8% between h50 and h10 and between h90 and h50, respectively, and the maximum increases of the mass-dependent SAFs in figure 17 are 16.8 and 10% between m50 and m10 and between m90 and m50, respectively. The SAFs(liver←lungs) in figure 14 decrease because inter-organ distances and organ masses increase with increasing height, with the difference in organ mass here being the dominant cause because liver and lungs are neighbouring organs. For a given target organ, further decrease of the SAF can be observed for source organs located at greater distance which is the case for the SAFs(liver←UBC) shown in figure 16.

Increase of body mass as modelled in this study leads to an increase of the adipose tissue surrounding the internal organs, thereby providing additional scatter material. This causes the SAFs in figure 15 to become greater with increasing body mass, a phenomenon already noted by Kim et al (2003) for the effective dose in case of external overhead exposure. In figure 17 one can observe that greater distance between source and target organ enhances this effect because more adipose scatter tissue is located along the way between source and target organ. Many photons scattered inwards by the adipose tissue of an obese person would have already left the body of a slim person.

4. Conclusions

The success of the CALDose_X software package (Kramer et al 2008) for calculating organ and tissue equivalent doses for patients submitted to X-ray examinations was one of the main incentives for this study because the ICRP89-based MASH3 and FASH3 phantoms, currently used in CALDose_X 4.0 (www.caldose.org), cannot represent all anatomies usually found among patients. Therefore, standing phantoms with different body masses and standing heights were developed which should improve organ and tissue equivalent dose calculations in the future. The world wide use of the CALDose_X software package was the reason for not choosing anthropometric data from a specific country but instead anthropometric data averaged over as many Caucasian populations as possible to define target parameters for the phantoms. As for the method of development, this study suggests to use updated anthropometric data for height and especially for body mass instead of the ICRP89 reference data to define the central phantoms. The use of the BMI to establish a link between body mass and standing height for the phantom development is considered to be acceptable because statistical correlation between the two anthropometric parameters is at best “modest” (Johnson et al 2009b). In this study for given standing height, organ masses in phantoms with different body masses were not changed because increase or decrease of body mass is considered to be mainly a result of changes of the subcutaneous adipose tissue mass. Of course, organ masses and/or positions can be different even in two persons having the same body mass and standing height, but how would one know?

Dosimetric results confirmed that for external exposure organ and tissue equivalent doses decrease with increasing body mass, for low energy exposure even dramatically, but only if the organ or tissue of interest is located below the subcutaneous adipose tissue layer. Otherwise, equivalent dose can remain constant or even increase with increasing body mass due to low attenuation and significant scatter effects. The results also confirmed the decrease of SAFs with increasing standing height, but also revealed that for a given height SAFs increase with increasing body mass due to radiation scattered in the increasing subcutaneous adipose tissue mass. The results suggest that changes of the body mass may have a significant effect on equivalent doses primarily for external exposure to organs and tissue located below the adipose tissue layer, while for superficial organs, for changes of the height and for internal exposures the effects on equivalent dose are small to moderate.

Obviously, with nine mass- and height-dependent phantoms per sex one cannot expect to match the enormous variety of anatomies found among patients, but together with the planned supine versions of the anthropometric phantoms one can hope to at least improve organ and tissue equivalent

dose calculations for X-ray diagnosis in the future. The use of the anthropometric phantoms is not restricted to medical applications. They can be used as well in the areas of occupational radiation protection or for equivalent dose estimate for members of the public especially for risk estimates when the use of the ICRP reference computational phantoms (ICRP 2009) is not appropriate.

5. Acknowledgements

The authors would like to thank the Conselho Nacional de Desenvolvimento Científico e Tecnológico - CNPq and the Fundação de Amparo à Ciência do Estado de Pernambuco - FACEPE for financial support.

6. References

- Alderson, S W, Lanzl, L H, Rollins, M and Spira, J (1962) An instrumented phantom system for analog computation of treatment plans, *Am J Roentg* **87** 185
- Azouz Z B, Rioux M, Shu C and Lepage R 2006 Characterizing human shape variation using 3D anthropometric data, *Visual Comput* **22** 302-314
- Cassola V F, de Melo Lima V J, Kramer R and Khoury H J 2010a FASH and MASH: Female and Male Adult human phantoms based on polygon meSH surfaces. Part I: Development of the anatomy *Phys Med Biol* **55** 133-162
- Cassola V F, Kramer R, Brayner C and Khoury H J 2010b Poster-specific phantoms representing female and male adults in Monte Carlo-based simulations for radiological protection *Phys Med Biol* **55** 4399-4430
- Clairand I, Bouchet L G, Ricard M, Durigon M, Di Paola M and Aubert B 2000 Improvement of internal dose calculations using mathematical models of different adult heights, *Phys Med Biol* **45** 2771-2785
- Clark L D, Stabin M G, Fernald M J and Brill A B 2010 Changes in radiation dose with variations on human anatomy: Moderately and severely obese adults, *J Nucl Med* **51** No 6 929-932
- De la Grandmaison G L, Clairand I and Durigon M 2001 Organ weight in 684 adult autopsies: new tables for a Caucasoid population, *Forensic Science International* **119** 149-154
- Divoli A, Chiavassa S, Ferrer L, Barbet J, Flux G D and Bardiès M 2009 Effect of patient morphology on dosimetric calculations for internal irradiation as assessed by comparisons of Monte Carlo versus conventional methodologies *J Nucl Med* **50** No 2 316-323
- Hartmann P, Ramseier A, Gudat F, Mihatsch M J, Polasek W and Geissenhoff C 1994 Das Normgewicht des Gehirns beim Erwachsenen in Abhängigkeit von Alter, Geschlecht, Körpergröße und Gewicht, *Pathologie* **15** 165-170
- Heymsfeld S B, Gallagher D, Mayer L, Beetsch J and Pietrobelli A 2007 Scaling of human body composition to stature: new insight into body mass index, *Am J Clin Nutr* **86** 82-91
- ICRP 2002 Basic Anatomical and Physiological Data for Use in Radiological Protection: Reference Values *ICRP Publication 89 (Oxford: Pergamon)*
- ICRP 2007 Recommendations of the International Commission on Radiological Protection *ICRP Publication 103 Ann. ICRP 37 (2-3) Elsevier Science Ltd., Oxford*
- ICRP 2009 Adult Reference Computational Phantoms *ICRP Publication 110 (Oxford: Pergamon)*
- Jeong J H, Cho S, Lee C, Cho K and Kim C 2008 Development of deformable computational model from Korean adult male based on polygon and NURBS surfaces *11th International Conference on Radiation Shielding, 13-18 April 2008, Callaway Gardens, Pine Mountain, Georgia, USA*
- Johnson P B, Lee C, Johnson K, Siragusa D and Bolch W E 2009a The influence of patient size on dose conversion coefficients: a hybrid phantom study for adult cardiac catheterization *Phys. Med. Biol.* **54** 3613-3629

- Johnson P B, Whalen S R, Wayson M, Juneja B, Lee C and Bolch W E 2009b Hybrid patient-dependent phantoms covering statistical distributions of body morphometry in the U.S. adult and pediatric population *Proc IEEE* **97** No 12 2060-2075
- Kim C H, Chichkov I and Reece W D 2003 Effect of torso adipose tissue thickness on effective dose in a broad parallel photon beam, *Health Phys* **85** No 4 471-475
- Kramer R 1979 Determination of conversion factors between organ equivalent doses and operational quantities for external exposure to X- and gamma rays, *Gesellschaft fuer Strahlen-und Umweltforschung, Muenchen-Neuherberg, GSF-Bericht-S-556*
- Kramer R, Khoury H J and Vieira J W 2008 CALDose_X a software tool for the assessment of organ and tissue doses, effective dose and cancer risk in diagnostic radiology *Phys Med Biol* **53** 6437-6459
- Kramer R, Cassola V F, Khoury H J, Vieira J W, de Melo Lima V J and Robson Brown K 2010 FASH and MASH: female and male adult human phantoms based on polygon mesh surfaces: II. Dosimetric calculations, *Phys Med Biol* **55** 163-189
- Lee C, Lodwick D, Hasenauer D, Williams J L, Lee C and Bolch W E 2007a Hybrid computational phantoms of the male and female newborn patient: NURBS-based whole-body models *Phys Med Biol* **52** 3309-3333
- Lee C, Lee C, Lodwick D and Bolch W E 2007b NURBS-based 3-D anthropomorphic computational phantoms for radiation protection dosimetry applications *Rad Prot Dos* **127** 227-232
- Lee C, Lodwick D, Williams J L and Bolch W E 2008 Hybrid computational phantoms of the 15-year male and female adolescent: Applications to CT organ dosimetry for patients of variable morphometry *Med Phys* **35**(6)2366-2382
- Lee C, Lodwick D, Hurtado J, Pafundi D, Williams J I and Bolch W E 2010 The UF family of reference hybrid phantoms for computational radiation dosimetry, *Phys Med Biol* **55** 339-363
- Li X, Samei E, Segars W P, Sturgeon G M, Colsher J G, Toncheva G, Yoshizumi T T and Frush D P 2011 Patient-specific radiation dose and cancer risk estimation in CT: Part II. Application to patients *Med Phys* **38** (1) 408-419
- Marine P M, Stabin M G, Fernald M J and Brill A B 2010 Changes in radiation dose with variations in human anatomy: Larger and smaller normal-stature adults *J Nucl Med* **51** No 5 806-811
- Na Y H, Zhang B, Zhang J, Caracappa P F and Xu X G 2010 Deformable adult human phantoms for radiation protection dosimetry: anthropometric data representing size distributions of adult worker populations and software algorithms, *Phys Med Biol* **55** 3789-3811
- Rannikko S, Ermakov I, Lampinen J S, Toivonen M, Karila K T K and Chervjakov A 1997 Computing patient doses of X-ray examinations using a patient size- and sex- adjustable phantom *Br J Radiol* **70** 708-718
- Sato K, Noguchi H, Endo A, Emoto Y, Kogs S and Saito K 2007 Development of a voxel phantom of Japanese adult male in upright position, *Rad Prot Dos* **127** (1-4) 205-208
- Sato K and Endo A 2008a Analysis of effects of posture on organ doses by internal photon emitters using voxel phantoms, *Phys Med Biol* **53** 4555-4572
- Sato K, Endo A and Kimiaki S 2008b Dose Conversion Coefficients Using a Series of Adult Japanese Voxel Phantoms against External Photon Exposure, *Japan Atomic Energy Agency, JAEA-DATA/Code 2008-016*
- Segars W P 2001 Development of a new dynamic NURBS-based cardiac-torso (NCAT) phantom, Ph.D. Thesis, University of North Carolina
- Servomaa A, Rannikko S, Nikitin V, Golikov V, Ermakov I, Masarskiy L and Saltukova L 1989 A topographically and anatomically unified phantom model for organ dose determination in radiation hygiene, Finish Centre for Radiation and Nuclear Safety, STUK-A87
- Snyder W S, Ford M R and Warner G G 1978 Estimates of absorbed fractions for monoenergetic photon sources uniformly distributed in various organs of a heterogeneous phantom, MIRD Pamphlet No.5, revised, Society of Nuclear Medicine, New York N. Y.
- Stabin M G, Sparks R B and Crowe E 2005 OLINDA/EXM: The Second-Generation Personal Computer Software for Internal Dose Assessment in Nuclear Medicine *J Nucl Med* **46**: 1023-1027

- Stabin M G, Emmons M A, Segars W P and Fernald M J 2009 The Vanderbilt University reference adult and pediatric phantom series. In: Xu X G, ed. Handbook of Anatomical Models for Radiation Dosimetry. Philadelphia, PA: Taylor & Francis, Inc. 337-346
- Tung C J, Lee C J, Tsai H Y, Tsai S F and Chen I J 2008 Body size-dependent patient effective dose for diagnostic radiology, *Radiation Measurement* **43** 1008-1011
- Veit R and Zankl M 1992 Influence of patient size on organ doses in diagnostic radiology, *Rad Prot Dos* **43**No 1/4 241-243
- Veit R and Zankl M 1993 Variation of organ doses in paediatric radiology due to patient diameter, calculated with phantoms of varying voxel size, *Rad Prot Dos* **49** Nos 1/3 353-356
- WinODS 2008 http://www.rti.se/download_software/index.html Accessed April 28, 2008
- Xu G, Taranenko V, Zhang J and Shi C 2007 A boundary-representation method for designing whole-body radiation dosimetry models: pregnant females at the end of three gestational periods – RPI-P3, -P6 and P9 *Phys Med Biol* **52** 7023-7044
- Xu X G, Zhang J Y and Na Y H 2008 Preliminary Data for Mesh-Based Deformable Phantom Development: Is it Possible to Design Person-Specific Phantoms On-demand. The International Conference on Radiation Shielding-11, April 14-17
- Zankl M, Panzer W and Herrmann C 2000 Calculation of patient doses using a human voxel phantom of variable diameter *Rad Prot Dos* **90** Nos 1-2 155-158
- Zhang J Y, Na Y H and Xu X G 2008a Size Adjustable Worker Models For Improved Radiation Protection Dosimetry. *Health Phys* **95**(1) S50
- Zhang J Y, Na Y H and Xu X G 2008b Development of Whole-Body Phantoms Representing An Average Adult Male and Female Using Surface-Geometry Methods, *Med Phys* **35**(6) 2875